ISSN: 3049-7272

Research Article

Journal of Biomedical Sciences and Biotechnology Research

Simulation-Based Evaluation of Signal-Quality Gating for Wearable Respiratory Monitoring During Procedural Sedation

Phan Minh Duc

Thai Binh High School for the Gifted, Vietnam

*Corresponding author
Phan Minh Duc, Thai Binh High School for the Gifted, Vietnam.

Received: October 12, 2026; **Accepted:** November 18, 2026; **Published:** November 27, 2026

ABSTRACT

Background: Motion artifacts and poor attachment can compromise chest-motion respiratory monitoring. This study evaluated the effect of a signal-quality gate on respiratory-rate estimates and motion-pause alerts.

Methods: The benchmark comprised 240 synthetic traces across six scenarios (40 per scenario), with two programmed pauses per trace (80 per scenario and 480 overall). Both algorithms processed identical traces and used the same rate estimator.

Results: Baseline and gated coverage were 89.7% and 46.2%, respectively. Mean absolute error (MAE) was 0.14 and 0.07 breaths/min on the respective sets of available estimates. All 1,830 shared rate estimates were identical. Pause sensitivity fell from 438/480 (91.25%) to 400/480 (83.33%), and false alerts fell from 100 to 20 over 12 hours (8.33 to 1.67 per hour). All 20 gated false alerts occurred in the shallow-motion scenario. During movement bursts, gating retained 16.0% of eligible rate windows and detected 0/80 pauses.

Conclusions: The gate reduced false alerts by selectively withholding output, with lower rate coverage and pause sensitivity. The findings apply to the six synthetic scenarios and identify conditions for subsequent physical bench testing.

Keywords: Respiratory Motion, Wearable Sensing, Computational Simulation, Signal Quality, Respiratory Rate, Pause Detection

Introduction

Respiratory monitoring during gastrointestinal endoscopy is motivated by the potential for decreased ventilatory drive and upper-airway obstruction during sedation. Clinical guidance considers sedation depth, patient characteristics and procedural context [1,2]. Chest movement provides a measurable signal for engineering studies, but respiratory effort can persist when airflow is obstructed. The proposed wearable therefore targets respiratory motion [3].

Contact-based respiratory sensing methods include inductive bands, impedance measurements, stretch sensors and inertial measurement units. Their sensitivity to attachment, posture and movement makes signal processing central to performance [3,4]. Rejecting difficult windows can lower the reported error while reducing the availability of rate estimates.

We processed identical synthetic chest-motion signals with a baseline algorithm and a version that applied quality gating. We compared rate error, coverage, false alerts and missed programmed pauses. A proposed wearable architecture provides the engineering context for the computational benchmark.

We asked how quality rejection changes error and availability, how it affects pause detection, and which disturbances reveal failures. The generator represents these challenges through scripted changes in rate, amplitude and continuity of cyclic motion. It omits sedative pharmacology, airway resistance, carbon dioxide dynamics and endoscopy workflow.

Citation: Phan Minh Duc. Simulation-Based Evaluation of Signal-Quality Gating for Wearable Respiratory Monitoring During Procedural Sedation. J Biomed Sci Biotech Res. 2026. 4(4): 1-6. DOI: doi.org/10.61440/JBSBR.2026.v4.48

Related Work and Design Rationale

Previous work describes chest-motion sensing and its susceptibility to motion artifacts [3,4]. ECG and photoplethysmography can also provide respiratory information, with different acquisition and artifact mechanisms [5]. This study used a single normalized motion channel to isolate the effect of rejection logic.

Weak respiratory motion and poor attachment can both yield low-amplitude signals. A quality rule that suppresses such intervals may also suppress events of interest. The benchmark includes programmed pauses and separate low-variance intervals representing contact loss.

The proposed architecture includes an inertial measurement unit, a battery-powered microcontroller, local timestamped storage and a status interface. A future implementation could record raw samples, quality flags and alert transitions. Risk management and usability guidance can inform subsequent physical development [6,7].

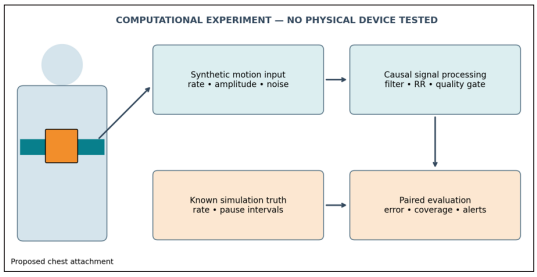

Figure 1: Proposed Device Context and Implemented Computational Evaluation. The Chest Attachment is an Engineering Illustration, not a Photograph of a Manufactured Prototype. All Numerical Results Derive from the Synthetic-input Branch

Materials and Methods

Study Design and Reproducibility

Each of six scenarios comprised 40 independently seeded traces of 180 s sampled at 25 Hz. The 240 traces represented 12 h of synthetic observation. Each trace contained two programmed motion pauses, giving 80 events per scenario and 480 overall. The two algorithms received the same trace in each run. The independently seeded run was the replication unit because analysis windows within a run overlapped.

Seeds followed seed = 20261105 + 1000s + k, with scenario index s = 0–5 in Table 1 order and replication index k = 0–39. NumPy default_rng was used for the generation, and SciPy was used for the filtering and peak detection. One fixed set of thresholds for the exploratory process was reported in the comparison. There was no threshold sweep or best-seed selection and thresholds were not externally calibrated.

Signal Generation

The generator combined phase-continuous periodic motion, low-frequency drift and independent Gaussian noise. The input is expressed in arbitrary units.

$$\varphi_i = 2\pi \Sigma_{j=0}^{i} (r_j / 60 f_s), \quad x_i = A_i \sin(\varphi_i) + 0.10 \sin(2\pi \times 0.025 t_i) + \varepsilon_i \qquad (1)$$

Here f_s = 25 Hz, $t_i = i/f_s$ and $\varepsilon_i \sim N(0, 0.045^2)$. Each run used an initial amplitude drawn from U (0.8, 1.2). The nominal rate was drawn from U (10, 22) breaths/min for all scenarios except Variable rate. In Variable rate, the nominal rate was 8, 18 and 28 breaths/min in successive 60 s blocks, with a single offset from U (−0.5, 0.5) breaths/min added to all three rates in each run. Table 1 specifies the additional scenario perturbations.

In all scenarios, respiratory amplitude was set to zero on [70, 86] and [125, 145] s, while drift and noise continued. In Movement bursts, some disturbances overlapped these pauses. During the two scripted loss-of-contact intervals in Loose contact, the complete observed signal was replaced by low-variance Gaussian noise. This model can favor variance-based rejection relative to physical attachment failures.

Table 1: Synthetic Test Matrix. Every Run also Contains Pauses at 70–86 and 125–145 s; no Human Data are Included

Scenario	Perturbation beyond common noise	Replications
Regular	Constant run-specific rate and amplitude	40
Variable rate	8, 18 and 28 breaths/min in successive 60 s blocks with a common run offset drawn from U(−0.5, 0.5)	40
Shallow motion	Amplitude ×0.20 at 35–60 and 95–120 s	40
Orientation shift	Amplitude ×0.35 from 90 s	40
Movement bursts	At 35–48, 78–91, 105–118 and 136–150 s: $N(0,0.65^2) + 0.8 \sin(2\pi \times 2t)$	40
Loose contact	Replace input by $N(0,0.012^2)$ at 40–58 and 100–117 s	40

Causal Processing and Respiratory Rate

A Butterworth bandpass filter designed using scipy.signal.butter with N = 2 and cutoffs of 0.08 and 0.70 Hz was applied from trace onset using forward filtering in second-order sections with zero initial conditions. Calibration amplitude B was the RMS of the filtered samples from 10 s up to but excluding 30 s. The first respiratory-rate estimate was evaluated at 30 s, after the calibration window was available.

$$B = \mathrm{RMS}(y_{10–30s}), \quad RR = 60 / \mathrm{median}[(p_{j+1} - p_j)/f_s] \qquad (2)$$

Rate was updated at 5 s intervals from 30 to 180 s using the preceding 20 s. Peaks required at least 1.2 s separation and prominence of at least 0.18B. At least three peaks were needed for an estimate. A window was eligible if it contained no programmed pause and its reference-rate range was below 2 breaths/min. Its reference rate was the mean programmed rate in that window. Coverage was calculated over these eligible windows.

Quality Gating and Pause Events

Let x denote the input, y the bandpass-filtered signal and z the input after a causal second-order Butterworth low-pass filter at 1

Hz, applied in second-order sections with zero initial conditions. For sample i at or after 2 s, RMS_2 and SD_2 are computed over the preceding 50 samples, excluding sample i. SD_2 uses the population standard deviation. Bracketed conditions take value 1 when true and 0 otherwise. For the first 50 samples, $L_i = 0$ and $g_i = 1$.

$$L_i = 1[RMS_2(y) < 0.22B],\ g_i = 1[RMS_2(x - z) < 0.30 \text{ and } SD_2(x) > 0.018] \quad (3)$$

For rate estimation, the gated algorithm required a baseline estimate, $g_i = 1$ for at least 90% of the samples in the 20 s window, and filtered-window RMS ≥ 0.22B. Estimates meeting these criteria were reported at their original value. For pause detection, the baseline used L_i and the gated algorithm used $L_i g_i$. An alert started after 250 consecutive qualifying samples (10 s) and ended when the condition failed. Filter settling and the trailing window contributed additional latency. In the offline benchmark, event detection scanned the full trace using the same B, including samples before 30 s. Event decisions before 30 s therefore used a calibration value that would only become available at 30 s in a streaming implementation

Each alert onset was matched chronologically to the first unmatched reference pause whose matching interval contained the onset. The interval extended from pause onset to 3 s after its end. Unmatched alerts counted as false alerts. Delay was measured from programmed onset to matched alert onset and averaged first within each run and then across runs with a match.

Outcomes and Uncertainty

$$MAE = \text{mean}(|\hat{RR} - RRref|),\ RMSE = \sqrt{\text{mean}[(\hat{RR} - RRref)^2]} \quad (4)$$

$$\text{Coverage} = 100N_{valid}/N_{eligible},\ \text{Sensitivity} = 100TP/(TP + FN) \quad (5)$$

$$\text{Precision} = 100TP/(TP + FP),\ \text{False-alert rate} = FP / \text{observation hours} \quad (6)$$

Rate error was calculated from available estimates and reported alongside coverage. False-alert rates used total observation hours, including programmed pauses. Bland–Altman plots show pooled bias and bias ± 1.96 SD [8]. The limits are descriptive because windows within a run overlap [9].

Overall, MAE and coverage intervals used 1,000 bootstrap resamples of 240 complete runs drawn with replacement from the combined scenario pool. All eligible windows from each selected run were carried into the resample. The random-number generator was initialized with seed 731 and advanced separately through each algorithms resamples. The percentile intervals describe variability within the specified simulation mixture. They do not quantify uncertainty across signal generators or support clinical inference.

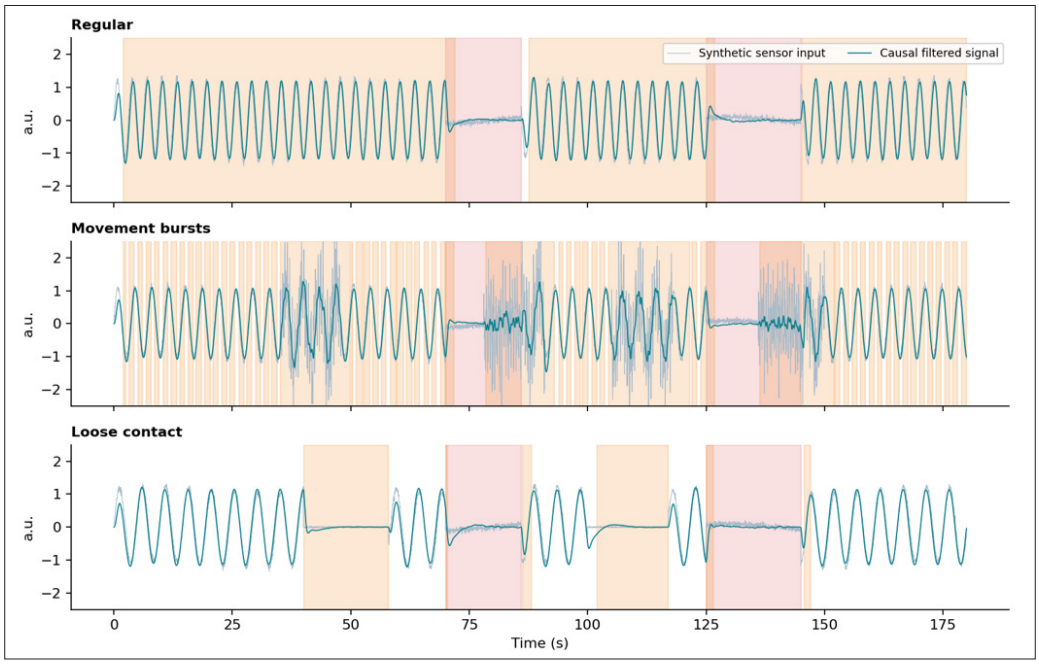

Figure 2: Three Representative Synthetic Runs. Red Shading Indicates Programmed Motion Pauses; Orange Shading Indicates Samples Rejected By the Quality Rule. Gray Input and Teal Filtered Traces Illustrate Artifact Overlap, Filter Settling and Contact-loss Ambiguity. Units are Arbitrary

Results

Respiratory Rate and Valid Output

Across 240 runs, each algorithm had 3,960 eligible rate windows. The baseline produced 3,554 estimates and the gated algorithm retained 1,830. MAE was 0.14 breaths/min (95% bootstrap interval 0.11–0.17) for baseline and 0.07 breaths/min (0.07–0.08) for gating. Coverage was 89.7% (87.7–91.8%) and 46.2% (41.8–51.2%), respectively. All 1,830 shared estimates were identical, so the pooled MAE difference reflects window selection. In Shallow motion, MAE on the respective available subsets increased from 0.12 to 0.13 breaths/min (Table 2).

Table 2: Rate Error in Breaths/min and Valid-output Coverage Among Eligible Windows. Each Scenario Contains 40 Independent Synthetic Runs

Scenario	Baseline MAE	Gated MAE	Baseline coverage	Gated coverage
Regular	0.05	0.04	100.0%	52.4%
Variable rate	0.07	0.04	73.2%	31.2%
Shallow motion	0.12	0.13	100.0%	63.8%
Orientation shift	0.07	0.07	100.0%	82.8%
Movement bursts	0.32	0.05	100.0%	16.0%
Loose contact	0.16	0.05	62.4%	28.4%

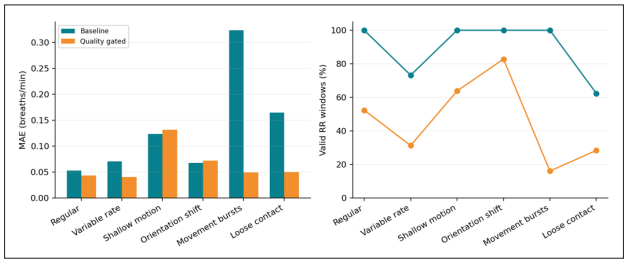

Figure 3: Mean Absolute Error and Valid-output Coverage are Shown for Each Scenario. Color Identifies Baseline and Gated Processing

Programmed Pauses and False Alerts

The baseline detected 438/480 programmed pauses (91.25%), and the gated algorithm detected 400/480 (83.33%). False alerts fell from 100 to 20 over 12 h, or from 8.33 to 1.67 per hour. Gating removed all 80 false alerts in Loose contact. The 20 false alerts in Shallow motion persisted with both algorithms. Precision increased from 81.4% to 95.2%. The mean run-level delay was 12.82 s for both algorithms among runs with matched alerts. In Movement bursts, the baseline detected 38/80 pauses and the gated algorithm detected 0/80 (Table 3 and Figure 4).

Table 3: Event Outcomes. B Denotes Baseline and G Quality Gated. Each Scenario Contributes 80 Pauses and Two Hours of Synthetic Observation. Sensitivity is a Percentage; Delay Averages Matched Events Only

Scenario	Sensitivity B / G	False alerts per hour B / G	Delay seconds B / G
Regular	100.0 / 100.0	0.00 / 0.00	12.95 / 12.95
Variable rate	100.0 / 100.0	0.00 / 0.00	12.73 / 12.73
Shallow motion	100.0 / 100.0	10.00 / 10.00	13.08 / 13.08
Orientation shift	100.0 / 100.0	0.00 / 0.00	12.30 / 12.30
Movement bursts	47.5 / 0.0	0.00 / 0.00	12.83 / N/A
Loose contact	100.0 / 100.0	40.00 / 0.00	13.04 / 13.04

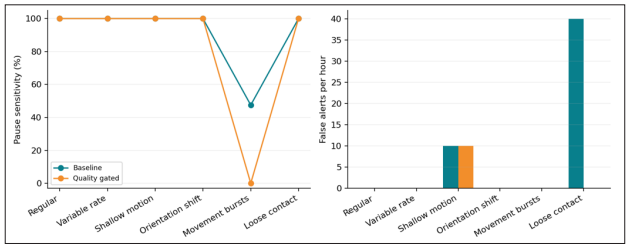

Figure 4: Pause sensitivity and false-alert burden under six synthetic conditions. Motion pauses are mathematical reference events, not verified episodes of clinical apnea

Descriptive Agreement

The pooled signed bias was 0.06 breaths/min for the baseline and nearly zero for the gated approach, while the RMSE values were 0.48 and 0.12, respectively. Figure 5 shows the signed error plotted against the paired mean. The discrete error bands arise from peak timing at a fixed sampling frequency and the use of median peak intervals. Both distributions are based on available synthetic estimates and should not be interpreted as evidence of clinical accuracy.

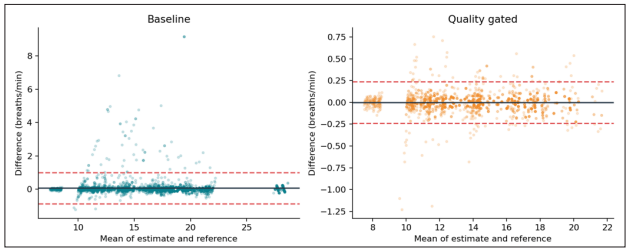

Figure 5: Descriptive Bland–Altman Displays for Available Synthetic Rate Windows. Solid Lines Show Pooled Bias; Dashed Lines Show Bias ±1.96 SD. Overlapping Windows are Dependent, and These Lines are not Clinical Acceptance Limits

Discussion

Meaning of the Computational Findings

The lower pooled MAE reflects which windows were retained. The estimator produced identical values on shared windows, and gating slightly increased the subset MAE in Shallow motion. The lower false-alert rate should be interpreted alongside reduced rate coverage and pause sensitivity.

In Regular, the gated algorithm retained 52.4% of eligible rate windows. The residual $x - z$ can include phase lag from the low-pass filter and may exceed the quality threshold even without an imposed disturbance. In Movement bursts, gating retained 16.0% of eligible rate windows and detected none of the 80 programmed pauses. Both findings motivate calibration against independent physical recordings.

The thresholds reflect the amplitudes and spectral separation of the simulated signals. Physical artifacts may overlap more strongly with the respiratory band or resemble physiological changes. The comparison evaluates one fixed gate under six specified scenarios.

Failure Mechanisms and Design Implications

Movement can interrupt the continuous low-amplitude evidence needed to trigger a pause alert. Severe attenuation can create

that evidence even when the reference shows continued motion. A future interface should indicate when output is unavailable because of suspected signal degradation.

The Orientation shift scenario approximated weaker coupling through scalar attenuation. A physical test would be needed to assess sensor rotation, gravitational projection and anatomical motion direction. Shallow motion represents amplitude reduction without a model of tidal volume or gas exchange.

Low cost is a design goal for the proposed architecture. Prototype evaluation would need to establish component and assembly costs, battery endurance, mass, comfort and cleaning compatibility.

Relevance to Procedural Monitoring

Procedural sedation motivates the choice of disturbances, but the benchmark evaluates chest-motion signals in software. Chest movement alone cannot establish airflow or effective ventilation. The proposed sensing approach would require separate clinical validation for procedural monitoring [1,2].

A bench study with an independent displacement reference could assess timing drift, sensor noise, attachment repeatability and the response to controlled disturbances. Any subsequent volunteer or clinical study would require an appropriate protocol, ethics review and consent [10]. Additional optical oxygen-saturation sensing would require independent validation [11]. Identifiable recordings would also require access and retention controls [12].

Limitations

The generator uses fixed pause times and fixed disturbance timing within scenarios. In Movement bursts, the same parts of the two pauses overlap with motion across all 40 runs. Independent random seeds vary signal and noise realizations under these assumptions. The observed sensitivity therefore applies to the tested overlap pattern. Future evaluation should vary event duration, relative timing and noise characteristics and test against physical recordings.

The study evaluated one fixed gate without component ablation or external validation. Rate agreement excludes pauses and transition windows, leaving dynamic rate tracking unassessed. Coverage is conditional on eligible windows, and false-alert rates use total observation time. Comparisons across available subsets are sensitive to the windows each algorithm retains.

Bootstrap intervals describe variability across synthetic runs. Pooled agreement limits are descriptive, and mean matched delay excludes missed events. Hardware, battery life, usability, electrical safety, cost and clinical performance remain unmeasured. The full-trace event scan evaluates offline detection. A streaming implementation would need to defer alerts until calibration is complete and verify the resulting performance.

Conclusion

Across six synthetic scenarios, quality gating reduced false alerts from 100 to 20 over 12 h (8.33 to 1.67 per hour), with all remaining false alerts occurring during shallow motion. Coverage fell from 89.7% to 46.2%, and pause detections fell from 438/480 to 400/480. During movement bursts, gating detected 0/80 pauses, compared with 38/80 at baseline. The lower overall MAE reflects selective retention of windows, with identical estimates on all 1,830 shared windows. Shallow-motion MAE increased from 0.12 to 0.13 breaths/min on the respective available subsets. These findings identify conditions for refining the gate and testing the proposed wearable architecture on a physical bench.

Declarations

Ethics and consent: No human participants, patient records, animal subjects or sedative administration were involved in the computational experiment described here. The analysis used generated signals only.

Data and code availability. The supplementary archive Respiratory_Simulation_Reproducibility.zip provides the signal-generation and analysis script, window-level estimates, run-level event outcomes, scenario summaries, bootstrap results and figures. All records are synthetic.

Appendix A Reproducibility Materials

Running simulation.py with the versions listed in requirements. txt regenerates the CSV outputs, bootstrap results and four result figures. The architecture illustration is provided separately in the same archive. An empty estimate field denotes unavailable output. Run identifiers refer to synthetic traces.

References

1. Early DS, Lightdale JR, Vargo JJ II, Acosta RD, Chandrasekhara V, et al. Guidelines for sedation and anesthesia in GI endoscopy. Gastrointest Endosc. 2018. 87: 327-337.
2. American Society of Anesthesiologists. Standards for basic anesthetic monitoring 2026.
3. Massaroni C, Nicolò A, Lo Presti D, Sacchetti M, Silvestri S, et al. Contact-based methods for measuring respiratory rate. Sensors. 2019. 19 :908.
4. Pecik M, Vavrinsky E, Vitazkova D, Kosnacova H, Nevrela J, et al. Respiratory monitoring in motion: an overview of wearable methods and algorithmic approaches for reliable assessment. Biosensors. 2026. 16 :306.
5. Charlton PH, Birrenkott DA, Bonnici T, Pimentel MAF, Johnson AEW, Alastruey J, et al. Breathing rate estimation from the electrocardiogram and photoplethysmogram: a review. IEEE Rev Biomed Eng. 2018. 11: 2-20.
6. International Organization for Standardization. ISO 14971:2019. Medical devices-Application of risk management to medical devices. Geneva: ISO. 2019. https://www.iso.org/standard/72704.html.
7. World Medical Association. WMA Declaration of Helsinki: ethical principles for medical research involving human participants 2024.
8. U.S. Food and Drug Administration. Applying human factors and usability engineering to medical devices: guidance for industry and Food and Drug Administration staff. 2026.
9. Bland JM, Altman DG. Statistical methods for assessing agreement between two methods of clinical measurement. Lancet. 1986. 327: 307-310.
10. Bland JM, Altman DG. Agreement between methods of

measurement with multiple observations per individual. J Biopharm Stat. 2007. 17: 571-582.
11. US. Food and Drug Administration. Pulse oximeters 2026.
12. Joint Task Force. Security and privacy controls for information systems and organizations. NIST Special Publication 800-53, Revision 5. Gaithersburg (MD): National Institute of Standards and Technology. 2020.

Copyright: © 2026 Phan Minh Duc. This is an open-access article distributed under the terms of the Creative Commons Attribution License, which permits unrestricted use, distribution, and reproduction in any medium, provided the original author and source are credited.